

PseudoNeg-MAE: Self-Supervised Point Cloud Learning using Conditional Pseudo-Negative Embeddings

Sutharsan Mahendren^{1,2}, Saimunur Rahman¹, Piotr Koniusz^{1,3},

Tharindu Fernando², Sridha Sridharan², Clinton Fookes², Peyman Moghadam^{1,2}

Abstract: We propose *PseudoNeg-MAE*, a novel self-supervised learning framework that enhances global feature representation of point cloud masked autoencoder by making them both discriminative and sensitive to transformations. Traditional contrastive learning methods focus on achieving invariance, discarding transformation-specific information. Recent approaches incorporate transformation sensitivity by explicitly modeling relationships between original and transformed inputs. However, they report an invariant-collapse phenomenon, where the predictor degenerates into identity mappings, resulting in latent representations that have limited variation across transformations. We propose a novel loss that explicitly penalizes invariant collapse, enabling the network to capture richer transformation cues while preserving discriminative representations. *PseudoNeg-MAE* uses a parametric network COPE, which learns the localized displacements caused by transformations within the latent space. However, jointly training COPE with the MAE leads to undesirable trivial solutions where COPE outputs collapse to an identity. To address this, we propose a loss that uses transformation-conditioned pseudo-negatives, to penalize such trivial invariant solutions. We validate *PseudoNeg-MAE* on shape classification and relative pose estimation tasks, where it achieves competitive performance on the ModelNet40 and ScanObjectNN datasets under challenging evaluation protocols and demonstrates superior accuracy in estimating relative poses compared to supervised methods.

Keywords: representation learning, point clouds, self-supervised learning

1 Introduction

Self-Supervised Learning (SSL) has emerged as a crucial approach in point cloud analysis, allowing models to learn robust and generalizable representations from large volumes of unlabeled 3D data. With the growing accessibility of affordable 3D sensors and scanning devices, point clouds have become a widely used data format in applications such as autonomous driving, robotics, and augmented reality. SSL methods have achieved remarkable success in various downstream tasks involving point clouds, including 3D object classification [1, 2, 3, 4], 3D scene understanding [5, 6], and 3D part segmentation [1, 2, 3, 4]. Traditional SSL methods, particularly those based on contrastive learning, focus on learning invariant representations to input perturbations or transformations. However, enforcing strict invariance to transformations may suppress critical geometric cues, such as orientation or spatial displacement, that are essential for tasks in robotics where the structure and dynamics of the physical world must be preserved.

¹CSIRO Robotics, DATA61, CSIRO, Australia. E-mails: *firstname.lastname@csiro.au*

²School of Electrical Engineering and Robotics, Queensland University of Technology (QUT), Brisbane, Australia.

³Australian National University

Recent approaches such as EquiMod [7] and SIE [8] address this limitation by introducing sensitivity to transformations (*i.e.*, equivariant objective), allowing models to explicitly encode the relationships between original and transformed point clouds in the latent space. SIE [8] shows that the linear predictor used by EquiMod [7] can suppress transformation channels, collapse into an identity mapping, and produce representations that are no more informative than those of purely invariant methods. To mitigate this shortcut, SIE replaces the linear layer with a bias-free hypernetwork whose weights are conditioned on the transformation. Although the hypernetwork conditions its weights on the transformation, it cannot guarantee that the predicted transformation deviates meaningfully from the identity. This limitation constrains the model’s ability to capture significant local displacements in the latent space. Consequently, the resulting representations may exhibit only limited variation in response to different transformations, reducing their sensitivity. This underscores the need for strong regularization mechanisms that actively promote responsiveness to transformations.

In this work, we propose a novel self-supervised learning framework, *PseudoNeg-MAE*, which learns transformation-sensitive representations while preserving discriminative capacity. Our key contribution is a loss function that bootstraps pseudo negatives conditioned on randomly sampled transformations, avoiding the risk of collapse to invariant solutions. These pseudo negatives serve as reference embeddings generated using the predictor, capturing the localized variations in the embedding space caused by different transformations. By incorporating them into the training objective, we encourage the model to produce representations that are sensitive to input transformations while avoiding degenerate solutions. To achieve this, we introduce the Conditional Pseudo Negatives EMBEDDING network (COPE). COPE takes transformation parameters as input and outputs a weight used to linearly project the original embeddings. This conditional mechanism enables the generation of transformation specific pseudo negatives. We use these pseudo negatives to regularize COPE through our proposed loss function, ensuring that distinct transformations yield sufficiently different embeddings in the latent space.

An advantage of our method is that it formulates relative pose estimation as an optimization problem in the embedding space, using transformation-sensitive features learned via the COPE. We introduce a novel inference algorithm that iteratively aligns source and target point cloud embeddings, achieving precise alignment even with large initial misalignments. We validate the effectiveness of *PseudoNeg-MAE* through comprehensive experiments on shape classification and relative pose estimation tasks. On the ModelNet40 and ScanObjectNN datasets, our method achieves state-of-the-art performance, particularly under challenging protocols. For relative pose estimation tasks, our framework excels in accurately estimating relative poses between point clouds, leading to superior performance compared to supervised baselines.

2 Related Works

Self-Supervised Learning for Point Cloud: Self-Supervised Learning (SSL) has become increasingly prevalent for leveraging unlabeled data, especially in the challenging domain of 3D point clouds. The inherent disorder and lack of predefined structure in point clouds necessitate diverse strategies for extracting meaningful representations. Among these, contrastive methods [6, 9, 1, 10] exploit correspondences across different views of point clouds to establish unsupervised pretraining frameworks using InfoNCE loss [11, 12]. In parallel, recent advancements have introduced transformer-based masked autoencoder approaches, such as PointBERT [13], which decodes discrete tokens from point patches, and PointMAE [3] along with PointM2AE [4], which directly predict the masked point patches rather than tokens. Extending this paradigm, Point2Vec [2] employs the principles of Data2vec [14] to facilitate feature space reconstruction in point clouds. Diverging from earlier SSL techniques that mainly induce biases towards invariant feature learning or local relationships for reconstruction, our approach focuses on learning both invariant and equivariant representations, significantly enhancing the performance across both downstream tasks.

Supervised Equivariant Networks: EPN [15] and E²PN [16] introduce SE(3)-equivariant architectures designed for point cloud analysis under supervised learning. EPN builds on KPConv [17]

by incorporating group convolutions over discretized $SO(3)$ to achieve rotation equivariance, while E^2PN [16] improves efficiency by using quotient representations on $S^2 \times \mathbb{R}^3$ with a permutation layer to recover full rotational structure. These models show strong performance on classification and relative pose estimation tasks but rely on labeled data. Additionally, Vector Neurons [18] represent another notable class of $SO(3)$ -equivariant networks, using vector-valued features that transform linearly under rotation. EquivReg [19] leverages Vector Neurons for correspondence-free point cloud registration, solving for relative rotations in closed-form within the equivariant feature space. Our method instead leverages the properties of equivariance as a self-supervisory signal for representation learning with a non-equivariant backbone, allowing for flexible training without labeled data while still benefiting from transformation-aware learning. We compare against these supervised baselines to highlight the advantages of our self-supervised framework.

Sensitivity to Transformation in SSL methods: Contrastive learning [12, 20, 21] has significantly advanced self-supervised representation learning; however, enforcing strict invariance to data augmentations can limit the expressive power of the learned features, especially in robotic tasks where details about specific transformations are crucial. To overcome this limitation, recent studies [22, 23, 7, 8] have explored enhancing models by incorporating sensitivity to transformations. One approach involves auxiliary tasks that require models to predict the transformations applied to the input data [24, 23, 22, 25], which helps preserve transformations-specific information within the representations and leads to less invariant feature spaces. However, these methods often lack guarantees of a consistent mapping between input transformations and changes in the latent representations [8]. Alternative approaches [26, 27], integrate loss functions that balance invariance with sensitivity to augmentations, enabling models to remain responsive to transformations while maintaining robustness. Additionally, recent methods [7, 8] have developed models that directly map transformations in the input space to transformations in the latent space, employing external predictors to modify representations accordingly. These methods [7, 8] identify the invariant-collapse problem, where predictors degenerate into identity mappings, effectively removing essential transformation cues from the learned representations. SIE [8] addresses this by replacing the linear predictor with a transformation-conditioned hypernetwork. However, without strong regularization, the predicted transformations of SIE can still converge toward the identity, leading to limited transformation sensitivity. In contrast, we introduce a novel penalty loss based on transformation-conditioned pseudo-negatives that explicitly discourages collapse into invariant representations and promotes responsiveness to transformations. Since EquiMod [7] and SIE [8] were originally developed for the image domain, we include additional experiments in the supplementary material evaluating our method against these baselines on image-based tasks. The results confirm that our proposed penalty loss effectively mitigates invariant collapse and enhances transformation sensitivity.

3 Proposed Approach - *PseudoNeg-MAE*

In this section, we introduce *PseudoNeg-MAE*, a method designed to learn feature representations that are both discriminative and sensitive to transformations. Our contrastive framework is built on the Masked AutoEncoder (MAE) transformer framework, combining the strengths of both predictive (MAE) and discriminative (contrastive) model training paradigms. As shown in Fig. 1, we model the relationship between input transformations and displacements in the embedding space using linear projections. These projections are controlled by a network, COPE, which generates transformation-specific weights. We train the main network f and COPE jointly. There is a risk that COPE could collapse into the identity matrix, producing invariant representations. To avoid this, we introduce a novel loss function that uses pseudo-negatives to regularize COPE and ensure that the projections are equivariant during training.

Let f be a parametric network that maps an input space \mathcal{X} to the unit sphere. Here f is a composition of an encoder \mathcal{E} and a decoder \mathcal{D} , (i.e., $f = \mathcal{E} \circ \mathcal{D}$). Let \mathcal{G} be a distribution of possible transformations in the input space \mathcal{X} , and g denotes a transformation sampled from the distribution \mathcal{G} . For the given input point cloud $\mathbf{x}_i \in \mathcal{X}$, g transforms it to a positive view $\mathbf{x}_i^+ = g(\mathbf{x}_i)$. The representations \mathbf{z} of $\mathbf{x}_i, \mathbf{x}_i^+$ is defined as $\mathbf{z}_i = f(\mathbf{x}_i)$ and $\mathbf{z}_i^+ = f(\mathbf{x}_i^+)$. Both \mathbf{z}_i and \mathbf{z}_i^+ reside within the same

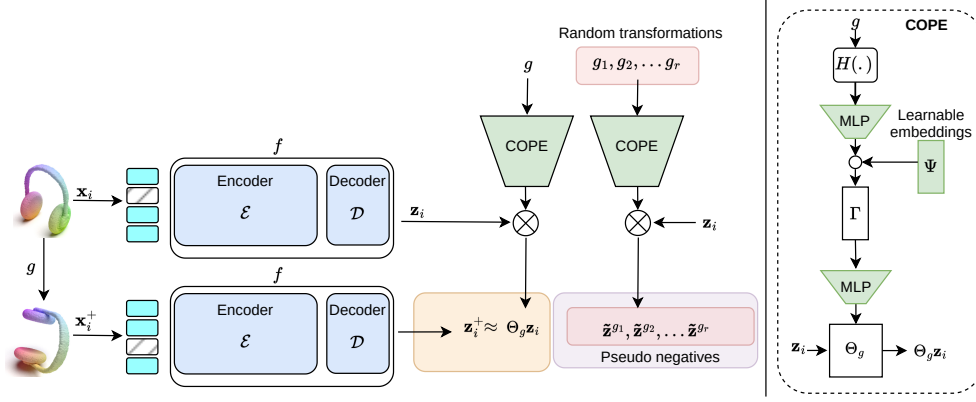


Figure 1: Overview of *PseudoNeg-MAE*: It encodes a point cloud \mathbf{x}_i and its transformed counter-part \mathbf{x}_i^+ , extracting their global representations \mathbf{z}_i and \mathbf{z}_i^+ , respectively, using a shared transformer architecture. Simultaneously, COPE network outputs the weight Θ_g and $\{\Theta_{g_r}\}$ based on the input and random transformations g and $\{g_r\}$. $\{\Theta_{g_r}\}$ are used to generate pseudo-negatives $\{\tilde{\mathbf{z}}_i^{g_r}\}$.

representation space \mathcal{Z} of f . We introduce an operator u_g that models how the transformation g affects the feature representation \mathbf{z}_i .

Contrastive learning methods, such as SimCLR [12], typically aim to learn a representation that is invariant to perturbations or transformations of the input data. This is achieved by encouraging similar instances to have similar representations in the embedding space, while dissimilar instances are pushed apart. This objective is equivalent to a combination of alignment $\mathcal{L}_{\text{align}}$ and uniformity $\mathcal{L}_{\text{unif}}$, as described in Eq. (1) below:

$$\mathcal{L}_{\text{align}} = \frac{1}{N} \sum_{i=1}^N \|\mathbf{z}_i - \mathbf{z}_i^+\|_2^2; \mathcal{L}_{\text{unif}} = \log \mathbb{E}_{(\mathbf{z}_i, \mathbf{z}_k) \sim \mathcal{Z} \times \mathcal{Z}} e^{-\|\mathbf{z}_i - \mathbf{z}_k\|_2^2 / \tau}; \mathcal{L}_{\text{ssl}} = \mathcal{L}_{\text{align}} + \mathcal{L}_{\text{unif}}. \quad (1)$$

Specifically, $\mathcal{L}_{\text{align}}$ promotes the invariance property, while $\mathcal{L}_{\text{unif}}$ regularizes the learning process by preventing dimensional collapse, where $f(x)$ becomes constant for all x [28]. Here τ is a temperature parameter. While invariant SSL models facilitate the learning process by discarding the variations introduced by transformations, they often neglect potentially critical information that these variations might carry. To address this issue, a group of self-supervised learning methods [7, 8, 26] has introduced the concept of *sensitivity to transformation*, enabling the model to explicitly encode the relationships between the original and augmented data in the latent space.

These approaches introduce a modified alignment term, $\mathcal{L}_{\text{align}}^* = \frac{1}{N} \sum_{i=1}^N \|u_g(\mathbf{z}_i) - \mathbf{z}_i^+\|_2^2$, where u_g defines the relationship between the feature representations \mathbf{z}_i and their augmented counterparts \mathbf{z}_i^+ under the transformation g . When combined with the uniformity term from Eq. (1), this alignment term helps the model avoid dimensional collapse while enhancing its sensitivity to transformations. A trivial solution to $\min_f \mathcal{L}_{\text{align}}^*$ is for all transformations $\forall g \in \mathcal{G}$ to collapse into the same embedding space (i.e., $u_g(\mathbf{z}_i) = \mathbf{z}_i$), making the embeddings invariant to transformations. To avoid this, our method, *PseudoNeg-MAE*, introduces an additional constraint that produces localized displacements in the embedding space, ensuring that: $u_{g_r}(\mathbf{z}_i) \neq u_{g_s}(\mathbf{z}_i)$; $(g_r, g_s) \sim \mathcal{G} \times \mathcal{G} : g_r \neq g_s$.

Sensitivity to Transformation through Pseudo Negatives: To effectively model the relationship u_g , we introduce Conditional Pseudo Negatives EMBEDDING (COPE) network based on hypernetworks [29, 8]. Specifically, COPE takes transformation parameter g as an input and outputs the weight $\Theta_g = \text{COPE}(g) \in \mathbb{R}^{d \times d}$. This weight is used as a linear projection on \mathbf{z}_i which learns the localized displacements due to the transformation g .

In our framework, COPE is jointly optimized with the main network f . Here, COPE learns to approximate the effect of transformations through its output weights Θ_g , while f must learn repre-

sentations \mathbf{z}_i and \mathbf{z}_i^+ that satisfy this linear constraint dependent on the transformations g . This is a challenging task because it requires f and COPE to closely cooperate.

A potential shortcut for COPE is to produce identity weights for all transformations, $\Theta_g = I$, making the features invariant to transformations. This trivial solution undermines our goal of learning transformation-sensitive representations. To avoid this, we introduce the process of *conditional generation of pseudo negatives* using COPE. With pseudo negatives, we regularize COPE and prevent it from collapsing into the identity. This approach ensures that different transformations produce different projections in the embedding, maintaining the sensitivity to the transformations. Specifically, we generate pseudo negatives by applying COPE to a set of randomly sampled transformations $\{g_r\}$ from \mathcal{G} , where $\{g_r\}$ are different from the input transformation g . For each g_r , the corresponding weight Θ_{g_r} with the COPE is computed and generated the pseudo negative embedding $\tilde{\mathbf{z}}_i^{g_r}$:

$$\tilde{\mathbf{z}}_i^{g_r} = \frac{\text{COPE}(g_r)\mathbf{z}_i}{\|\text{COPE}(g_r)\mathbf{z}_i\|} = \frac{\Theta_{g_r}\mathbf{z}_i}{\|\Theta_{g_r}\mathbf{z}_i\|}. \quad (2)$$

We incorporate these pseudo negatives into our novel loss function $\mathcal{L}_{\text{cope}}$ to regularize COPE.

$$\mathcal{L}_{\text{cope}} = \frac{1}{N} \sum_{i=1}^N \log \left[\sum_{r=1}^M e^{-\left\| \frac{\Theta_{g_r}\mathbf{z}_i}{\|\Theta_{g_r}\mathbf{z}_i\|} - \tilde{\mathbf{z}}_i^{g_r} \right\|_2^2 / \tau} + e^{-\left\| \frac{\Theta_g\mathbf{z}_i}{\|\Theta_g\mathbf{z}_i\|} - \mathbf{z}_i^+ \right\|_2^2 / \tau} \right], \quad (3)$$

where M is the number of pseudo negatives. This loss penalizes the model for mapping different transformations to similar embeddings, thus preventing the trivial solution. Consider the case of perfect alignment where $\mathbf{z}_i^+ = \frac{\Theta_g\mathbf{z}_i}{\|\Theta_g\mathbf{z}_i\|}$. Minimizing $\mathcal{L}_{\text{cope}}$ is equivalent to optimizing $\log \left[\sum_{r=1}^M e^{-\left\| \frac{\Theta_{g_r}\mathbf{z}_i}{\|\Theta_{g_r}\mathbf{z}_i\|} - \tilde{\mathbf{z}}_i^{g_r} \right\|_2^2 / \tau} + 1 \right]$, which effectively maximizes the pairwise distances between $\{\Theta_{g_r}\mathbf{z}_i\}$. Achieving this requires diverse $\{\Theta_{g_r}\}$ from the COPE, thereby penalizing trivial invariant solutions. We define the final loss $\mathcal{L}_{\text{PseudoNegMAE}}$ as follows:

$$\mathcal{L}_{\text{PseudoNegMAE}} = \mathcal{L}_{\text{align}^*} + \beta \mathcal{L}_{\text{cope}} + (1 - \beta) \mathcal{L}_{\text{unif}}. \quad (4)$$

Specifically, $\mathcal{L}_{\text{unif}}$ encourages discriminative features and $\mathcal{L}_{\text{cope}}$ preserves the sensitivity to transformations within the feature space. This combination enables the model to learn discriminative and sensitive representations to input transformations. The loss $\mathcal{L}_{\text{align}^*}$ encourages the positive \mathbf{z}_i to be pulled towards the anchor. $\mathcal{L}_{\text{cope}}$ encourages the pseudo negatives $\tilde{\mathbf{z}}_i^{g_r}$ to be pushed away from the anchor $\frac{\Theta_g\mathbf{z}_i}{\|\Theta_g\mathbf{z}_i\|}$. For a given \mathbf{z}_i all the pseudo-negatives $\{\Theta_{g_r}\mathbf{z}_i\}$ only depend on the output of the COPE Θ_{g_r} network. This avoids Θ_g collapsing into identity, preventing the undesired invariant solution. Unlike SIE [8] whose equivariance is mainly enforced through an alignment loss, a term that trivially vanishes when the predictor collapses to the identity, $\mathcal{L}_{\text{COPE}}$ conditioned with the Pseudo-Negatives reaches its maximum when predictor collapse to identity. The full proof appears in the Supplementary Materials.

COPE Network Architecture: COPE generates linear weights conditioned on the transformation set $\{g\}$. In our work, we consider rotations as transformations and utilize quaternions to represent them as inputs to the COPE. The network architecture is illustrated in the right section of Fig. 1. First, we embed g into a harmonic space $H(\cdot)$, using a set of high-frequency functions [30]. Subsequently, these embedded quaternions are processed through an MLP network to extract transformation-sensitive embeddings, denoted as $\mathbf{h}'_g \in \mathbb{R}^{\frac{d}{k}}$. Independently estimating each element of Θ_g is computationally expensive. Therefore, we utilize shared learnable embedding vectors $\Psi \in \mathbb{R}^{\frac{d}{k} \times d}$, which are responsible for the entries of the rows in Θ_g . We perform an element-wise multiplication of these vectors with our \mathbf{h}'_g , i.e., $\Gamma = \mathbf{h}'_g \odot \Psi$, where $\Gamma \in \mathbb{R}^{d \times \frac{d}{k}}$. A shared non-linear MLP network is then used to expand each column of Γ to the dimension d . This process yields the linear weight $\Theta_g \in \mathbb{R}^{d \times d}$. Consequently, Θ_g is determined solely based on the input transformation.

We generate pseudo negatives using COPE by sampling a set of random rotations $\{g_r\}_{r=1}^M$. We uniformly sample quaternions representing 3D rotations to ensure coverage over the rotation space. Specifically, for each pseudo negative, we generate a random vector $\mathbf{v}_r = (w_r, x_r, y_r, z_r)$ by sampling from a standard normal distribution $\mathbf{v}_r \sim \mathcal{N}(0, I_4)$. We then normalize \mathbf{v}_r to obtain a unit

quaternion g_r and ensure the scalar part is nonnegative: $g_r = \frac{\mathbf{v}_r}{|\mathbf{v}_r|} \cdot \text{sign}(w_r)$. This approach ensures that the set of quaternions g_r is uniformly distributed over the space of 3D rotations. Random rotations are fed to the COPE for generating pseudo negatives as in Eq. 2.

PseudoNeg-MAE Transformer Backbone: Our contrastive framework is built on the Masked AutoEncoder (MAE), combining the strengths of both predictive (MAE) and discriminative (contrastive) model training paradigms. We employ a shared Siamese encoder with a point cloud transformer backbone f , initialized with weights from an MAE in which there are two branches with shared weights. *PseudoNeg-MAE* operates on pairs of point clouds: a randomly sampled point cloud \mathbf{x}_i and its transformed point cloud \mathbf{x}_i^+ with the applied transformation g . Following the standard transformer architecture on the point cloud, we first extract a sequence of non-overlapping point patches, which are then converted to a set of tokens.

Given an input point cloud \mathbf{x} , we first used Furthest Point Sampling (FPS) to sample a set of n center points. Then, K Nearest-Neighbour (KNN) is utilized to select k neighboring points around each center point to construct n point patches. Following this, patch tokens are generated using a mini-PointNet [3] and fed to the transformer encoder. However, in *PseudoNeg-MAE*, not all the patch tokens are processed by the encoder. A random masking strategy is applied independently to \mathbf{x}_i and \mathbf{x}_i^+ , masking m number of the point patches. Only visible tokens are fed to an encoder (\mathcal{E}). This independent masking strategy encourages the learning of representations that are robust to noise and occlusions. Then, the encoded embeddings of visible tokens from the two inputs are sent to the decoders with shared weights. An extra learnable [CLS] token is appended to each encoder output. We implement a lightweight decoder \mathcal{D} . The objective of the decoder is to aggregate the encoder outputs into representations \mathbf{z}_i and \mathbf{z}_i^+ .

Relative Pose Estimation Using COPE: To tackle the challenge of relative pose estimation between source and target point clouds, we introduce a novel algorithm that utilizes the COPE network to optimize the transformation parameters directly. The algorithm focuses on estimating the quaternions to minimize the difference between the transformed source and target embeddings, thus achieving precise alignment.

The process, detailed in Algorithm 1, starts by exploring a set of randomly generated quaternions $\{g_r\}$, representing potential rotations between the source and target. Each quaternion is evaluated in a bi-directional manner—applying the transformation to both the source and the target embeddings via g_r and g_r^{-1} . Here g_r^{-1} is the inverse of g_r . The quaternions are refined through an iterative process, where each is adjusted according to the gradient update weighted by $\epsilon = 0.01$. After updating the quaternions, it is essential to ensure they remain valid unit quaternions, which is achieved by the normalization step at line 9. The quaternion associated with the minimum loss is designated as g_{est} serving as the final solution for the alignment. This process ensures that the iterative refinement systematically approaches the global minimum of the loss landscape. In summary, this algorithm extends the capabilities of COPE to solve relative pose estimation by optimizing quaternions to align global embeddings of point clouds.

4 Results

We evaluate our model on downstream tasks, specifically shape classification and relative pose estimation for both objects and scene levels, to demonstrate the advantage of the invariant and equivariant properties of our approach. Details of our hyperparameters and pre-training settings are given in the Supplementary Materials.

Shape Classification: We evaluate our model on two prominent 3D object classification datasets, namely, ModelNet40 and ScanObjectNN. ModelNet40 [43] consists of 12,311 clean 3D CAD models from 40 categories, split into 9,843 instances for training and 2,468 for testing. ScanObjectNN [44] is a more challenging dataset derived from real-world indoor scenes containing approximately 15,000 objects across 15 categories.

Algorithm 1: Transformation Estimation with COPE.

Data: Source and target $\mathbf{z}_{src}, \mathbf{z}_{tgt}$

```

1 Initialize  $\mathcal{L}_{\min} = \infty$ ;
2 for  $j = 1 \dots N_{out}$  do
3   Initialise  $g_r = (w_r, x_r, y_r, z_r)$ ;
4   for  $k = 1 \dots N_{in}$  do
5      $\mathbf{z}^{g_r} = \frac{\text{COPE}(g_r)\mathbf{z}_{src}}{\|\text{COPE}(g_r)\mathbf{z}_{src}\|}$ ;
6      $\mathbf{z}^{g_r^{-1}} = \frac{\text{COPE}(g_r^{-1})\mathbf{z}_{tgt}}{\|\text{COPE}(g_r^{-1})\mathbf{z}_{tgt}\|}$ ;
7      $\mathcal{L}_{g_r} = \frac{1}{2} \|\mathbf{z}_{tgt} - \mathbf{z}^{g_r}\|_2^2 + \frac{1}{2} \|\mathbf{z}_{src} - \mathbf{z}^{g_r^{-1}}\|_2^2$ ;
8      $g_r \leftarrow g_r - \epsilon \nabla_{g_r} \mathcal{L}_{g_r}$ ;
9      $g_r \leftarrow \frac{g_r}{\|g_r\|} \text{sign}(w_r)$ ;
10  end
11  if  $\mathcal{L}_{g_r} < \mathcal{L}_{\min}$  then
12     $\mathcal{L}_{\min} \leftarrow \mathcal{L}_{g_r}, g_{est} \leftarrow g_r$ ;
13  end
14 end
15 return  $g_{est}$ 

```

Table 1: Shape classification results on ModelNet40 dataset and ScanObjNN’s OBJ-BG subset under z/z and S0(3)/SO(3) evaluation scenario.

Method	ModelNet40		ScanObjNN
	z/z	SO(3)/SO(3)	SO(3)/SO(3)
Supervised			
PointNet [31]	89.2	75.5	54.7
PoinNet++ [31]	89.3	85.0	47.4
PCT [32]	90.3	88.5	45.8
SFCNN [33]	91.4	90.1	–
RIConv [34]	86.5	86.4	78.1
RI-GCN [35]	89.5	89.5	80.6
GCACNN [36]	89.0	89.2	80.3
RI-Framework [37]	89.4	89.3	79.9
VN-DGCNN [38]	89.5	90.2	80.3
OrientedMP [39]	88.4	88.9	77.2
Yu et al. [40]	91.0	91.0	86.3
PaRot [41]	90.9	90.8	82.6
LocoTrans [42]	91.6	91.5	84.5
Self-Supervised Learning			
PointMAE [3]	90.7	89.3	83.3
Point2Vec [2]	91.3	88.4	84.7
PseudoNeg-MAE	92.5	91.1	89.0

We follow the protocols of [45] for the evaluation in Tab. 1: z/z – training and testing under rotations around the z-axis and SO(3)/SO(3) – training and testing under the arbitrary 3D rotations. Tab. 1 provides a detailed comparison of different point cloud backbones applied to the ModelNet40 and ScanObjectNN datasets across different protocols. The table is divided into sections detailing Supervised and SSL approaches. Here supervised section consists of equivariant methods [33] - [42] which are designed to handle rotations. Our SSL-based model, *PseudoNeg-MAE*, achieves superior performance on ModelNet40 and ScanObjNN, outperforming all supervised and self-supervised methods under S0(3)/SO(3) on challenging ScanObjNN *OBJ-BG* by a considerable margin, and ModelNet40 under z/z while remaining highly competitive under S0(3)/SO(3). This demonstrates that our novel pretraining approach enhances the generalization capabilities across diverse ranges.

Relative Pose Estimation: We assess our model on relative pose estimation benchmark tasks, where the goal is to predict the relative rotation between pairs of point clouds. We fine-tune the network f and COPE using $\mathcal{L}_{\text{align}^*}$ and $\mathcal{L}_{\text{cope}}$, and conduct inference following Algorithm 1. The evaluation is conducted under two scenarios: object-level and scene-level point clouds. We use the mean isotropic rotation error [46] for the evaluation.

Object Level: In the object-level evaluation, we utilize five categories from the ModelNet40 dataset, following the protocol established by EPN [15]. We present both quantitative and qualitative evaluations in Tab. 2 and Fig. 2, respectively. Our self-supervised model, *PseudoNeg-MAE*, shows the best overall performance compared to supervised counterparts, including both non-equivariant (such as KPConv [17]) and equivariant (EPN [15] and E²PN [16]) networks. By achieving lower maximum rotation errors across all categories, *PseudoNeg-MAE* demonstrates its superior ability to learn

Table 2: Relative pose estimation results over five categories with E²PN protocol. Here, all the other compared methods are supervised. Among them, KPConv is a non-equivariant method while EPN and E²PN are equivariant networks. Our self-supervised approach performs better than the supervised equivariant methods.

Learning Type	Mean / Max / Med (°)	Airplane	Bottle	Car	Chair	Sofa
Supervised Learning	KPConv [17]	12.0 / 70.5 / 10.0	8.0 / 104.4 / 5.0	35.8 / 175.6 / 20.9	26.0 / 168.3 / 16.3	84.2 / 177.3 / 75.2
	EPN [15]	1.3 / 6.2 / 1.1	1.2 / 22.3 / 0.8	2.6 / 117.6 / 1.1	1.2 / 9.0 / 1.0	1.5 / 15.0 / 1.1
	E ² PN [16]	1.5 / 11.1 / 1.1	1.9 / 46.1 / 1.1	3.3 / 74.0 / 1.5	2.9 / 38.2 / 1.8	2.7 / 33.6 / 1.9
Self-Supervised Learning	PseudoNeg-MAE	0.8 / 2.2 / 0.8	1.7 / 9.6 / 0.8	1.4 / 3.7 / 1.3	1.5 / 5.8 / 1.4	1.2 / 4.0 / 1.1

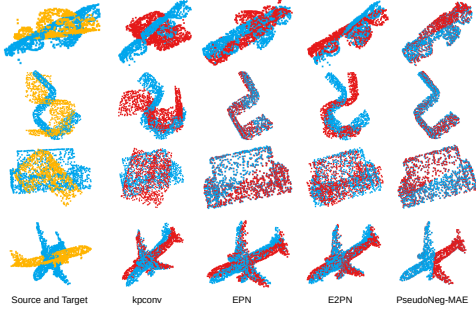


Figure 2: Illustration of relative pose estimation between source (yellow) and target (blue) point clouds for KPCConv, EPN, E^2 PN, and *PseudoNeg-MAE*. Red indicates transformed source clouds.

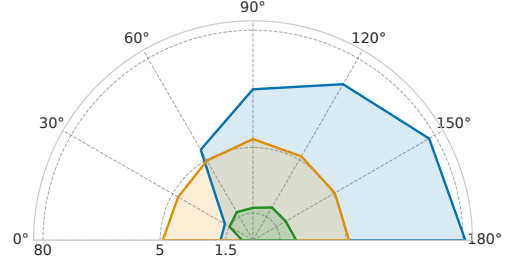


Figure 3: Relative pose estimation on 7Scenes under varying maximum rotational angles (logarithmic scale for better visualization). FMR [47], EquivReg [19], *PseudoNeg-MAE*.

robust rotation-sensitive embeddings. This helps to significantly enhance the alignment accuracy of point clouds, validating the effectiveness of our proposed method in handling all ranges of rotations.

Scene Level: In addition to the object-level evaluation, we extend our analysis to relative pose estimation at the scene level using the 7Scenes dataset, a real-world indoor dataset that is a subset of 3DMatch [48]. This dataset features over 100,000 points per scene. We sample 1024 points to form the source and target point clouds. We compare our method with correspondence-free pose estimation methods where FMR [47] is an iterative approach and EquivReg [19] uses an equivariant encoder. Following the protocol described in EquivReg [19], we generate random rotations by uniformly sampling the angles with the specified maximum ($0^\circ, \dots, 180^\circ$), alongside randomly selected rotation axes, to compute rotation errors. The findings are summarized in Fig. 3 with a logarithmic scale for better visualization. It shows the *PseudoNeg-MAE*’s ability to maintain consistent lower error across the range of angles.

5 Conclusion

In this paper, we proposed *PseudoNeg-MAE*, a novel self-supervised learning framework aimed at preventing collapse to invariant solutions in contrastive learning for point cloud data. Our approach introduces a loss function that leverages pseudo-negatives, ensuring that the learned representations remain both discriminative and sensitive to transformations. We also presented a novel inference algorithm for relative pose estimation, which utilizes the transformation-sensitive feature space and COPE network to iteratively estimate the relative pose between point clouds. We conducted extensive experiments on shape classification and relative pose estimation tasks, which demonstrate that *PseudoNeg-MAE* outperforms existing methods, especially in challenging rotation scenarios. For relative pose estimation tasks, our framework excels in accurately estimating relative poses between point clouds, leading to superior performance compared to supervised baselines.

6 Limitation

In this work, we primarily analyze 3D rotations as the transformation of interest. Extending *PseudoNeg-MAE* to other transformation types such as scaling, translation, or deformation, and modeling their combined effects, remains an important direction for future work. Additionally, our approach assumes a linear relationship in the feature space caused by transformations, which may not fully capture complex or non-rigid transformation behaviors. Addressing these limitations could further improve the generality and expressiveness of our framework.

References

- [1] M. Afham, I. Dissanayake, D. Dissanayake, A. Dharmasiri, K. Thilakarathna, and R. Rodrigo. Crosspoint: Self-supervised cross-modal contrastive learning for 3d point cloud understanding. In *Proceedings of the IEEE/CVF Conference on Computer Vision and Pattern Recognition*, pages 9902–9912, 2022.
- [2] K. Abou Zeid, J. Schult, A. Hermans, and B. Leibe. Point2vec for self-supervised representation learning on point clouds. In *German Conference on Pattern Recognition (GCPR)*, 2023.
- [3] Y. Pang, W. Wang, F. E. Tay, W. Liu, Y. Tian, and L. Yuan. Masked autoencoders for point cloud self-supervised learning. In *European conference on computer vision*, pages 604–621. Springer, 2022.
- [4] R. Zhang, Z. Guo, P. Gao, R. Fang, B. Zhao, D. Wang, Y. Qiao, and H. Li. Point-m2ae: Multi-scale masked autoencoders for hierarchical point cloud pre-training. In *Adv. Neural Inform. Process. Syst. (NeurIPS)*, 2022.
- [5] X. Zhan, X. Pan, Z. Liu, D. Lin, and C. C. Loy. Self-supervised learning via conditional motion propagation. In *IEEE/CVF Conference on Computer Vision and Pattern Recognition (CVPR)*, pages 1881–1889, 2019.
- [6] S. Xie, J. Gu, D. Guo, C. R. Qi, L. Guibas, and O. Litany. Pointcontrast: Unsupervised pre-training for 3d point cloud understanding. In *European conference on computer vision*, pages 574–591, 2020.
- [7] A. DEVILLERS and M. Lefort. Equimod: An equivariance module to improve visual instance discrimination. In *The Eleventh International Conference on Learning Representations*, 2023.
- [8] Q. Garrido, L. Najman, and Y. Lecun. Self-supervised learning of split invariant equivariant representations. In *International Conference on Machine Learning*. PMLR, 2023.
- [9] Z. Zhang, R. Girdhar, A. Joulin, and I. Misra. Self-supervised pretraining of 3d features on any point-cloud. In *Proceedings of the IEEE/CVF International Conference on Computer Vision*, pages 10252–10263, 2021.
- [10] A. Sanghi. Info3d: Representation learning on 3d objects using mutual information maximization and contrastive learning. In *European conference on computer vision*, pages 626–642, 2020.
- [11] A. v. d. Oord, Y. Li, and O. Vinyals. Representation learning with contrastive predictive coding. *arXiv preprint arXiv:1807.03748*, 2018.
- [12] T. Chen, S. Kornblith, M. Norouzi, and G. Hinton. A simple framework for contrastive learning of visual representations. In *Proceedings of the 37th International Conference on Machine Learning*, pages 1597–1607, 2020.
- [13] X. Yu, L. Tang, Y. Rao, T. Huang, J. Zhou, and J. Lu. Point-bert: Pre-training 3d point cloud transformers with masked point modeling. In *Proceedings of the IEEE/CVF Conference on Computer Vision and Pattern Recognition*, pages 19313–19322, 2022.
- [14] A. Baevski, W.-N. Hsu, Q. Xu, A. Babu, J. Gu, and M. Auli. Data2vec: A general framework for self-supervised learning in speech, vision and language. In *International Conference on Machine Learning*, pages 1298–1312. PMLR, 2022.
- [15] H. Chen, S. Liu, W. Chen, H. Li, and R. Hill. Equivariant point network for 3d point cloud analysis. In *Proceedings of the IEEE/CVF conference on computer vision and pattern recognition*, pages 14514–14523, 2021.

- [16] M. Zhu, M. Ghaffari, W. A. Clark, and H. Peng. E2pn: Efficient se (3)-equivariant point network. In *Proceedings of the IEEE/CVF Conference on Computer Vision and Pattern Recognition*, pages 1223–1232, 2023.
- [17] H. Thomas, C. R. Qi, J.-E. Deschaud, B. Marcotegui, F. Goulette, and L. J. Guibas. Kpconv: Flexible and deformable convolution for point clouds. In *Proceedings of the IEEE/CVF international conference on computer vision*, pages 6411–6420, 2019.
- [18] C. Deng, O. Litany, Y. Duan, A. Poulenard, A. Tagliasacchi, and L. J. Guibas. Vector neurons: A general framework for so (3)-equivariant networks. In *Proceedings of the IEEE/CVF International Conference on Computer Vision*, pages 12200–12209, 2021.
- [19] M. Zhu, M. Ghaffari, and H. Peng. Correspondence-free point cloud registration with so (3)-equivariant implicit shape representations. In *Conference on Robot Learning*, pages 1412–1422. PMLR, 2022.
- [20] K. He, H. Fan, Y. Wu, S. Xie, and R. Girshick. Momentum contrast for unsupervised visual representation learning. In *2020 IEEE/CVF Conference on Computer Vision and Pattern Recognition (CVPR)*, 2020.
- [21] J. Knights, S. Hausler, S. Sridharan, C. Fookes, and P. Moghadam. GeoAdapt: Self-supervised test-time adaptation in lidar place recognition using geometric priors. *IEEE Robotics and Automation Letters*, 9(1):915–922, 2024.
- [22] R. Dangovski, L. Jing, C. Loh, S. Han, A. Srivastava, B. Cheung, P. Agrawal, and M. Sol-jacic. Equivariant self-supervised learning: Encouraging equivariance in representations. In *International Conference on Learning Representations*, 2022.
- [23] H. Lee, K. Lee, K. Lee, H. Lee, and J. Shin. Improving transferability of representations via augmentation-aware self-supervision. *Advances in Neural Information Processing Systems*, 34:17710–17722, 2021.
- [24] S. Gidaris, P. Singh, and N. Komodakis. Unsupervised representation learning by predicting image rotations. In *International Conference on Learning Representations*, 2018.
- [25] F. Scherr, Q. Guo, and T. Moraitis. Self-supervised learning through efference copies. *Advances in Neural Information Processing Systems*, 35:4543–4557, 2022.
- [26] S. Gupta, J. Robinson, D. Lim, S. Villar, and S. Jegelka. Structuring representation geometry with rotationally equivariant contrastive learning. In *International Conference on Learning Representations*, 2024.
- [27] J. Wang, Y. Chen, and S. X. Yu. Pose-aware self-supervised learning with viewpoint trajectory regularization. *European Conference on Computer Vision*, 2024.
- [28] T. Wang and P. Isola. Understanding contrastive representation learning through alignment and uniformity on the hypersphere. In *International conference on machine learning*, pages 9929–9939, 2020.
- [29] D. Ha, A. M. Dai, and Q. V. Le. Hypernetworks. In *International Conference on Learning Representations*, 2017.
- [30] B. Mildenhall, P. P. Srinivasan, M. Tancik, J. T. Barron, R. Ramamoorthi, and R. Ng. Nerf: Representing scenes as neural radiance fields for view synthesis. *Communications of the ACM*, pages 99–106, 2021.
- [31] C. R. Qi, H. Su, K. Mo, and L. J. Guibas. Pointnet: Deep learning on point sets for 3d classification and segmentation. In *Proceedings of the IEEE conference on computer vision and pattern recognition*, pages 652–660, 2017.

- [32] M.-H. Guo, J.-X. Cai, Z.-N. Liu, T.-J. Mu, R. R. Martin, and S.-M. Hu. Pct: Point cloud transformer. *Computational Visual Media*, 7:187–199, 2021.
- [33] Y. Rao, J. Lu, and J. Zhou. Spherical fractal convolutional neural networks for point cloud recognition. In *Proceedings of the IEEE/CVF conference on computer vision and pattern recognition*, pages 452–460, 2019.
- [34] Z. Zhang, B.-S. Hua, D. W. Rosen, and S.-K. Yeung. Rotation invariant convolutions for 3d point clouds deep learning. In *2019 International conference on 3d vision (3DV)*, pages 204–213. IEEE, 2019.
- [35] S. Kim, J. Park, and B. Han. Rotation-invariant local-to-global representation learning for 3d point cloud. *Advances in Neural Information Processing Systems*, 33:8174–8185, 2020.
- [36] Z. Zhang, B.-S. Hua, W. Chen, Y. Tian, and S.-K. Yeung. Global context aware convolutions for 3d point cloud understanding. In *2020 International Conference on 3D Vision (3DV)*, pages 210–219. IEEE, 2020.
- [37] X. Li, R. Li, G. Chen, C.-W. Fu, D. Cohen-Or, and P.-A. Heng. A rotation-invariant framework for deep point cloud analysis. *IEEE transactions on visualization and computer graphics*, 28(12):4503–4514, 2021.
- [38] H. Deng, T. Birdal, and S. Ilic. Ppfnet: Global context aware local features for robust 3d point matching. In *Proceedings of the IEEE conference on computer vision and pattern recognition*, pages 195–205, 2018.
- [39] S. Luo, J. Li, J. Guan, Y. Su, C. Cheng, J. Peng, and J. Ma. Equivariant point cloud analysis via learning orientations for message passing. In *Proceedings of the IEEE/CVF Conference on Computer Vision and Pattern Recognition*, pages 18932–18941, 2022.
- [40] J. Yu, C. Zhang, and W. Cai. Rethinking rotation invariance with point cloud registration. In *Proceedings of the AAAI Conference on Artificial Intelligence*, volume 37, pages 3313–3321, 2023.
- [41] D. Zhang, J. Yu, C. Zhang, and W. Cai. Parot: Patch-wise rotation-invariant network via feature disentanglement and pose restoration. In *Proceedings of the AAAI Conference on Artificial Intelligence*, pages 3418–3426, 2023.
- [42] Y. Chen, L. Duan, S. Zhao, C. Ding, and D. Tao. Local-consistent transformation learning for rotation-invariant point cloud analysis. In *Proceedings of the IEEE/CVF Conference on Computer Vision and Pattern Recognition*, pages 5418–5427, 2024.
- [43] Z. Wu, S. Song, A. Khosla, F. Yu, L. Zhang, X. Tang, and J. Xiao. 3d shapenets: A deep representation for volumetric shapes. In *Proceedings of the IEEE conference on computer vision and pattern recognition*, pages 1912–1920, 2015.
- [44] M. A. Uy, Q.-H. Pham, B.-S. Hua, T. Nguyen, and S.-K. Yeung. Revisiting point cloud classification: A new benchmark dataset and classification model on real-world data. In *Proceedings of the IEEE/CVF international conference on computer vision*, pages 1588–1597, 2019.
- [45] C. Esteves, C. Allen-Blanchette, A. Makadia, and K. Daniilidis. Learning so (3) equivariant representations with spherical cnns. In *Proceedings of the European Conference on Computer Vision (ECCV)*, pages 52–68, 2018.
- [46] Z. J. Yew and G. H. Lee. Rpm-net: Robust point matching using learned features. In *IEEE/CVF Conference on Computer Vision and Pattern Recognition (CVPR)*, pages 11824–11833, 2020.
- [47] X. Huang, G. Mei, and J. Zhang. Feature-metric registration: A fast semi-supervised approach for robust point cloud registration without correspondences. In *The IEEE/CVF Conference on Computer Vision and Pattern Recognition (CVPR)*, June 2020.

- [48] A. Zeng, S. Song, M. Nießner, M. Fisher, J. Xiao, and T. Funkhouser. 3dmatch: Learning local geometric descriptors from rgb-d reconstructions. In *IEEE/CVF Conference on Computer Vision and Pattern Recognition (CVPR)*, pages 1802–1811, 2017.
- [49] J. Y. Park, O. Biza, L. Zhao, J. W. van de Meent, and R. Walters. Learning symmetric representations for equivariant world model. In *International Conference on Machine Learning*, 2022.
- [50] A. X. Chang, T. Funkhouser, L. Guibas, P. Hanrahan, Q. Huang, Z. Li, S. Savarese, M. Savva, S. Song, H. Su, et al. Shapenet: An information-rich 3d model repository. *arXiv preprint arXiv:1512.03012*, 2015.
- [51] Z. Jiang, Y. Chen, M. Liu, D. Chen, X. Dai, L. Yuan, Z. Liu, and Z. Wang. Layer grafted pre-training: Bridging contrastive learning and masked image modeling for label-efficient representations. In *The Eleventh International Conference on Learning Representations*, 2023.
- [52] M. Haghighat, P. Moghadam, S. Mohamed, and P. Koniusz. Pre-training with Random Orthogonal Projection Image Modeling. In *The Twelfth International Conference on Learning Representations*, 2024.

Supplementary Material

PseudoNeg-MAE: Self-Supervised Point Cloud Learning using Conditional Pseudo-Negative Embeddings

1 Degenerate identity predictor is a global optimum for the SIE loss

In this subsection, we demonstrate that the SIE loss [8] admits a trivial global optimum where the predictor collapses to the identity mapping and the encoder outputs invariant, non-collapsed features. Specifically, we show that this degenerate solution achieves minimum loss, thus failing to prevent the collapse to trivial invariance. In contrast, our proposed loss function, incorporating pseudo-negatives explicitly, penalizes such identity-predictor collapse. We prove that our loss attains the maximum (in contrast to the minimum), precisely under the degenerate identity solution, enforcing the model to learn non-trivial, transformation-sensitive representations.

To formalize this, consider the case in which:

1. The predictor collapses to the identity mapping, and
2. The encoder produces *invariant, non-collapsed* features.

SIE objective. Given an encoder $f_\theta : \mathcal{X} \rightarrow \mathbb{R}^d$ and a predictor $\rho_\psi : \mathcal{G} \rightarrow \text{GL}(d)$, the SIE loss for a pair of views $(x_i, x'_i) = (x_i, g_i \cdot x_i)$ decomposes into

$$\begin{aligned} \mathcal{L}_{\text{SIE}} = & \underbrace{\mathcal{L}_{\text{reg}}(Z) + \mathcal{L}_{\text{reg}}(Z')}_{\text{regularization}} + \underbrace{\lambda_{\text{inv}} \frac{1}{N} \sum_{i=1}^N \|Z_{i,\text{inv}} - Z'_{i,\text{inv}}\|_2^2}_{\mathcal{L}_{\text{inv}}} \\ & + \underbrace{\lambda_{\text{eq}} \frac{1}{N} \sum_{i=1}^N \|\rho_\psi(g_i) Z_{i,\text{eq}} - Z'_{i,\text{eq}}\|_2^2}_{\mathcal{L}_{\text{equiv}}} + \underbrace{\lambda_V V(\rho_\psi(g_i) Z_{i,\text{eq}})}_{\mathcal{L}_{\text{stab}}}, \end{aligned} \quad (5)$$

where $Z_i = f_\theta(x_i) = [Z_{i,\text{inv}}, Z_{i,\text{eq}}]$.

$$\mathcal{L}_{\text{reg}}(Z) = \lambda_C C(Z) + \lambda_V V(Z), \quad \text{with}$$

$$C(Z) = \frac{1}{d} \sum_{i \neq j} \text{Cov}(Z)_{i,j}^2, \quad \text{and}$$

$$V(Z) = \frac{1}{d} \sum_{j=1}^d \max \left(0, 1 - \sqrt{\text{Var}(Z_{\cdot,j})} \right).$$

Constructing the degenerate solution. Assume there exists an encoder $f_{\theta^*}(\cdot)$ that outputs *invariant* but non-collapsed features:

$$\underbrace{f_{\theta^*}(x_i)}_{Z_i} = \underbrace{f_{\theta^*}(g_i \cdot x_i)}_{Z'_i} =: Z_i^* \quad \forall x_i, g_i \in \mathcal{G}. \quad (C1)$$

Because the features are non-collapsed, each dimension has above unit variance and zero cross-covariance, hence $C(Z^*) = V(Z^*) = 0$.

Let the predictor collapse to the identity,

$$\rho_{\psi^*}(g) = I_d \quad \forall g \in \mathcal{G}. \quad (C2)$$

- **Regularization.** $\mathcal{L}_{\text{reg}}(Z_i^*) = 0$ by construction.
- **Invariant term.** $Z_{i,\text{inv}}^* = Z_{i,\text{inv}}^{*'} \implies \mathcal{L}_{\text{inv}} = 0$.
- **Equivariant term.** $\rho_{\psi^*}(g_i) = I_d$ gives $\mathcal{L}_{\text{equiv}} = \frac{\lambda_{\text{eq}}}{N} \sum_i \|Z_{i,\text{eq}}^* - Z_{i,\text{eq}}^{*'}\|_2^2 = 0$.
- **Stability term.** Because $V(Z_i^*) = 0$, also $V(\rho_{\psi^*}(g_i)Z_{i,\text{eq}}^*) = V(I_d Z_{i,\text{eq}}^*) = 0$.

Every component of (5) therefore vanishes, so $\mathcal{L}_{\text{SIE}}(\theta^*, \psi^*) = 0$. Hence an identity predictor together with fully invariant features is a (global) minimizer of the SIE objective

2 Our Loss Penalizes Predictor Collapse

Here we verify that the same degenerate configuration (θ^*, ψ^*) is *not* optimal for our objective. Fig. 4 conceptually illustrates our objective, where for each input embedding \mathbf{z}_i , we generate an anchor $\frac{\Theta_{g_i} \mathbf{z}_i}{\|\Theta_{g_i} \mathbf{z}_i\|}$ using its corresponding transformation g_i , along with multiple pseudo-negatives $\tilde{\mathbf{z}}_i^{g_r}$, each corresponding to a random transformation g_r . Here \mathbf{z}_i and \mathbf{z}_i^+ are the embeddings of original and the transformed inputs, both normalized to unit norm. Both the anchor and pseudo-negatives are generated by our predictor COPE, parameterized by ψ .

Our overall objective is defined as:

$$\mathcal{L}_{\text{PseudoNegMAE}} = \mathcal{L}_{\text{align}^*} + \beta \mathcal{L}_{\text{cope}} + (1 - \beta) \mathcal{L}_{\text{unif}}, \quad (6)$$

$$\mathcal{L}_{\text{align}^*} = \frac{1}{N} \sum_{i=1}^N \left\| \frac{\Theta_{g_i} \mathbf{z}_i}{\|\Theta_{g_i} \mathbf{z}_i\|} - \mathbf{z}_i^+ \right\|_2^2, \quad (7)$$

$$\mathcal{L}_{\text{unif}} = \log \mathbb{E}_{(\mathbf{z}_i, \mathbf{z}_k) \sim \mathcal{Z} \times \mathcal{Z}} e^{-\|\mathbf{z}_i - \mathbf{z}_k\|_2^2 / \tau}, \quad (8)$$

where $\Theta_{g_i} = \text{COPE}_{\psi}(g_i)$,

Alignment and uniformity. Conditions (C1),(C2) drive the alignment loss to its minimum, $\mathcal{L}_{\text{align}^*} = 0$, and likewise minimize $\mathcal{L}_{\text{unif}}$.

The COPE term resists collapse.

$$\mathcal{L}_{\text{cope}} = \frac{1}{N} \sum_{i=1}^N \log \left[\sum_{r=1}^M \exp \left(-\frac{\left\| \frac{\Theta_{g_i} \mathbf{z}_i}{\|\Theta_{g_i} \mathbf{z}_i\|} - \tilde{\mathbf{z}}_i^{g_r} \right\|_2^2}{\tau} \right) + \exp \left(-\frac{\left\| \frac{\Theta_{g_i} \mathbf{z}_i}{\|\Theta_{g_i} \mathbf{z}_i\|} - \mathbf{z}_i^+ \right\|_2^2}{\tau} \right) \right] \quad (9)$$

Here $\tilde{\mathbf{z}}_i^{g_r} = \frac{\Theta_{g_r} \mathbf{z}_i}{\|\Theta_{g_r} \mathbf{z}_i\|}$ are pseudo negatives corresponding to random transformation g_r .

$$\mathcal{L}_{\text{cope}} = \frac{1}{N} \sum_{i=1}^N \log \left[\sum_{r=1}^M \exp \left(-\frac{\left\| \frac{\Theta_{g_i} \mathbf{z}_i}{\|\Theta_{g_i} \mathbf{z}_i\|} - \frac{\Theta_{g_r} \mathbf{z}_i}{\|\Theta_{g_r} \mathbf{z}_i\|} \right\|_2^2}{\tau} \right) + \exp \left(-\frac{\left\| \frac{\Theta_{g_i} \mathbf{z}_i}{\|\Theta_{g_i} \mathbf{z}_i\|} - \mathbf{z}_i^+ \right\|_2^2}{\tau} \right) \right] \quad (10)$$

We substitute $\Theta_{g_i} = \Theta_{g_r} = I_d$ to simulate the collapse case: Here the predictor COPE outputs the same identity weight for every transformation.

$$\mathcal{L}_{\text{cope}} = \frac{1}{N} \sum_{i=1}^N \log \left[M + \exp \left(-\frac{\left\| \frac{\mathbf{z}_i}{\|\mathbf{z}_i\|} - \mathbf{z}_i^+ \right\|_2^2}{\tau} \right) \right] \quad (11)$$

As $\|\mathbf{z}_i\| = 1$, we have:

$$\mathcal{L}_{\text{cope}} = \frac{1}{N} \sum_{i=1}^N \log \left[M + \exp \left(-\frac{\|\mathbf{z}_i - \mathbf{z}_i^+\|_2^2}{\tau} \right) \right] \quad (12)$$

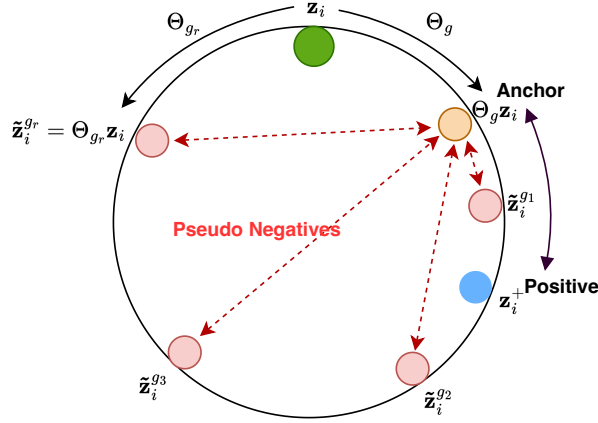


Figure 4: Conceptual visualization of the loss $\mathcal{L}_{\text{PseudoNeg-MAE}}$. Using COPE, we generate the anchor $\frac{\Theta_g \mathbf{z}_i}{\|\Theta_g \mathbf{z}_i\|}$ and a set of pseudo negatives $\frac{\Theta_{g_r} \mathbf{z}_i}{\|\Theta_{g_r} \mathbf{z}_i\|}$ for the corresponding positive \mathbf{z}_i^+ . As per our main goal, due to these pseudo negatives, the model remains sensitive to different transformations rather than becoming completely invariant to them.

Under the Condition (C1), where the encoder is invariant, \mathbf{z}_i and \mathbf{z}_i^+ are equal. Therefore, we have:

$$\mathcal{L}_{\text{cope}} = \frac{1}{N} \sum_{i=1}^N \log \left[\sum_{r=1}^M 1 + 1 \right] = \log(M + 1),$$

For any predictor outputs satisfying

$$\Theta_{g_r} \neq \Theta_g \quad \text{for all } r = 1, \dots, M,$$

$$\left\| \frac{\Theta_{g_i} \mathbf{z}_i}{\|\Theta_{g_i} \mathbf{z}_i\|} - \frac{\Theta_{g_r} \mathbf{z}_i}{\|\Theta_{g_r} \mathbf{z}_i\|} \right\|_2^2 > 0 \implies -\frac{\left\| \frac{\Theta_{g_i} \mathbf{z}_i}{\|\Theta_{g_i} \mathbf{z}_i\|} - \frac{\Theta_{g_r} \mathbf{z}_i}{\|\Theta_{g_r} \mathbf{z}_i\|} \right\|_2^2}{\tau} < 0 \quad (13)$$

$$\exp \left(-\frac{\left\| \frac{\Theta_{g_i} \mathbf{z}_i}{\|\Theta_{g_i} \mathbf{z}_i\|} - \frac{\Theta_{g_r} \mathbf{z}_i}{\|\Theta_{g_r} \mathbf{z}_i\|} \right\|_2^2}{\tau} \right) < 1 \implies \sum_{r=1}^M \exp \left(-\frac{\left\| \frac{\Theta_{g_i} \mathbf{z}_i}{\|\Theta_{g_i} \mathbf{z}_i\|} - \frac{\Theta_{g_r} \mathbf{z}_i}{\|\Theta_{g_r} \mathbf{z}_i\|} \right\|_2^2}{\tau} \right) < M \quad (14)$$

$$\mathcal{L}_{\text{cope}} < \log(M + 1). \quad (15)$$

$\mathcal{L}_{\text{COPE}}$ becomes its maximum when the predictor collapses to identity. Hence our loss explicitly penalizes the identity-predictor degeneration, forcing the optimizer to learn a non-trivial, transformation sensitive mapping.

The above analysis shows that SIE alone cannot prevent the identity solution, whereas the COPE term in $\mathcal{L}_{\text{PseudoNegMAE}}$ introduces a penalty that impose the learning dynamics towards equivariant representations.

3 Comparisons with SOTA Equivariant Representation Learning Methods in Image Domain

In this experiment, we rigorously evaluate our proposed $\mathcal{L}_{\text{PseudoNegMAE}}$ and its predictor module COPE against existing state-of-the-art equivariant representation learning methods in the image domain. Specifically, we compare our approach with SEN [49], EquiMod [7], and SIE [8] on the established 3D Invariant-Equivariant Benchmark (3DIEBench) [8]. As *PseudoNeg-MAE* is originally developed for point clouds, we adapt it to the image domain and ensure a fair evaluation by using the same ResNet-18 backbone architecture across all methods.

Dataset: For evaluation in the image domain, we use the 3D Invariant-Equivariant Benchmark (3DIEBench) introduced by Garrido *et al.* [8]. 3DIEBench is specifically designed to evaluate both invariant and equivariant properties of learned representations. It contains over 2.5 million images generated by rendering 52,472 objects from ShapeNetCore [50] across 55 categories under a diverse set of 3D rotations. We follow the protocol established in SIE [8] and use the provided image splits without modification. This setup allows consistent evaluation across tasks such as classification and rotation prediction, where the objective is to assess how well representations capture class-specific discriminative features and transformation sensitivity.

Table 3: Quantitative evaluation of learned representations on invariant (classification) and equivariant (rotation prediction) tasks. For fair comparison, we adopt *PseudoNeg-MAE** by adding our proposed loss and predictor module to a ResNet-18 backbone, following the same architecture used in prior works.

Method	Classification (top-1)	Rotation prediction (R^2)
SEN* [49]	86.93	0.51
EquiMod [7]	87.19	0.47
SIE [8]	82.94	0.73
<i>PseudoNeg-MAE*</i>	87.7	0.74

Classification and rotation prediction: We follow the protocol of SIE in 3DIEBench dataset and assess representation quality on image classification and rotation prediction tasks. For classification, we train a linear classifier on frozen representations, and for rotation prediction, we regress the transformation between two views using a 3-layer MLP. As shown in Table 3, *PseudoNeg* outperforms prior methods, achieving the highest top-1 classification accuracy (87.70%) and R^2 score for rotation prediction (0.74), indicating strong discriminative features and transformation sensitivity.

Table 4: Quantitative evaluation on MRR, H@1, and H@5 metrics.

Method	MRR (\uparrow)	H@1 (\uparrow)	H@5 (\uparrow)
EquiMod [7]	0.16	0.05	0.22
SEN* [49]	0.17	0.05	0.22
SIE [8]	0.41	0.30	0.51
<i>PseudoNeg-MAE*</i>	0.54	0.41	0.69

Predictor Evaluation via Image Retrieval: To evaluate the effectiveness of our predictor, we adopt the retrieval-based metrics introduced in SIE: Mean Reciprocal Rank (MRR), Hit Rate at 1 and 5 (H@1, H@5). Given a source embedding and the known transformation, we apply the learned predictor and retrieve the nearest neighbours among views of the same object. MRR measures the average inverse rank of the ground-truth target, while H@k reports if the target appears within the top-k neighbours. As reported in Table 4, *PseudoNeg-MAE** achieves superior retrieval performance (MRR = 0.54, H@1 = 0.41, H@5 = 0.69), significantly outperforming EquiMod and SIE. This confirms that our pseudo-negative formulation avoids predictor collapse and promotes a more transformation-aware embedding space.

Notably, our predictor achieves these results using only 200K learnable parameters, which is significantly fewer than the 4 million parameters required by the SIE predictor. This efficiency is enabled by our use of a shared MLP across the columns of the predicted weight matrix in the COPE architecture. In contrast, SIE predicts all d^2 elements of the transformation matrix independently from the rotation parameters, leading to substantially higher model complexity.

Qualitative evaluation on predictor accuracy To qualitatively evaluate the accuracy of the localized displacement caused by the predictor of our proposed method, *PseudoNeg-MAE**, we conduct

Table 5: Performance comparison for varying numbers of pseudo-negatives, where zero pseudo-negatives corresponds to the absence of the $\mathcal{L}_{\text{cope}}$ loss ($\beta = 0$).

Evaluation	Classification (top-1 %)	Rotation prediction (R^2)
0 (w/o $\mathcal{L}_{\text{cope}}$)	87.5	0.533
16	88.0	0.726
32	87.6	0.738
64	87.7	0.740

a nearest-neighbor retrieval analysis in the embedding space. Specifically, given a source object, the task involves predicting embeddings corresponding to the transformation of the target object using the predictor. Retrieval of the nearest neighbors of these predicted embeddings is performed across a search space comprising images from all classes, with the expectation that the retrieved neighbors closely match the target’s pose and category.

Fig. 5 compares our method to SIE through representative examples. Results indicate that embeddings generated by SIE predictor frequently retrieve nearest neighbors that mismatch in either pose or category. In contrast, embeddings from our proposed *PseudoNeg-MAE** consistently exhibit superior alignment, closely matching both the pose and category of the target object. These results highlight the improved performance of the COPE predictor in modeling transformation-specific displacements and demonstrate the effectiveness of PseudoNeg-MAE in learning transformation-sensitive representations.

Effect of Pseudo-Negatives. To evaluate the role of pseudo-negatives in our proposed loss, we perform an ablation by varying their number while keeping the rest of the setup fixed. As shown in Table 5, removing the $\mathcal{L}_{\text{cope}}$ term (i.e., using zero pseudo-negatives) results in a substantial drop in rotation prediction performance ($R^2 = 0.533$), highlighting the importance of explicitly penalizing transformation sensitivity. In contrast, incorporating pseudo-negatives significantly improves rotation prediction, reaching an R^2 of 0.740 with 64 negatives, while maintaining high classification accuracy (87.7%). These results demonstrate that our loss formulation effectively encourages equivariant representations without compromising discriminative features.



Figure 5: Nearest neighbours of predicted embeddings: Given the source embedding and the transformation to the target, each method’s predictor generates a predicted embedding whose top-3 nearest neighbours (NN1–NN3) are shown.

4 Pre-training and implementation details of *PseudoNeg-MAE* with point cloud

Table 6: Pretraining hyperparameters for *PseudoNeg-MAE*.

Config	Value
Optimizer	AdamW
Weight decay	0.05
Learning rate	1×10^{-3}
LR schedule	Cosine annealing with linear warmup
Warmup epochs	80
Batch size	512
Training epochs	1600
β	0.3
Encoder depth	12
Num. pseudo-negatives	8

We initialize the encoder \mathcal{E} of our network f using a point cloud MAE [2] and pretrain with our contrastive formulation. The proposed *PseudoNeg-MAE* is a modular component that integrates with any point cloud MAE backbone. We follow the procedure utilized in Masked Autoencoders for images [51, 52] as an effective way of integrating the contrastive objective with mask reconstruction pre-training. We use the training set of the ShapeNet dataset [50], which contains approximately 42,000 synthetic point clouds across 55 object categories for training. We sample 1024 points from each point cloud for pretraining.